Development of Highly Transparent Polypropylene Sheets

AKIRA FUNAKI [a], TOSHITAKA KANAI [a], KANAME KONDO [b], HIROSHI ODAKA [b]*

[a]*Performance Materials Laboratories, Idemitsu Kosan Co., Ltd*
1-1, Anesaki-Kaigan, Ichihara, Chiba, 299-0193, Japan
[b] *R&D Center for Plastic Products, Idemitsu Unitech Co., Ltd.*
1660, Kamiizumi, Sodegaura, Chiba, 299-0205, Japan

Abstract. In order to obtain highly transparent isotactic polypropylene (PP) sheets by an industrial process, various factors contributing to transparency were analyzed. At first, the observation was experimentally conducted by using many screws with various geometries. The transparency of melted web was obtained by the screw geometry so that the specific energy consumption was small. Then the higher order structure of the higher tacticity PP sheets was investigated. After the heat treatment of quick quenched sheets, the matrix was transformed from smectic structure to α-monoclinic crystal phase. The density and refractive index differences between spherulite and matrix were decreased, and the transparency was drastically improved. Additionally, the influence of the isotacticity, molecular weight distribution, crystallization control material and multilayer extrusion process were analyzed. The lower tacticity PP generated the less and the smaller size of spherulites and showed the improvement behavior on transparency by heat treatment. In the case of addition of L-LDPE with the specific density to PP, the transparency was markedly improved by the heat treatment. This phenomenon could be explained by the refractive index difference of PP matrix and the fine distribution particles of L-LDPE. The shear stress was reduced by laminating resin with low melt viscosity on both surfaces, and therefore it can be surmised that the stress induced crystallization was restrained.

1. INTRODUCTION

There have been a lot of researches in the past for the higher order of quenched isotactic polypropylene sheet [1-10]. It is well known that a highly transparent sheet of a crystalline polypropylene resin can be obtained by quick quenching a molten resin sheet in the laboratories. There are mainly two theories in terms of higher order structure which is formed during its solidification process. One is the crystallization theory of bulk polymers with chain folding based on the nucleation of spherulites and then the growth through the molecular diffusion of spherulites by Hoffman et al. [11]. Other is a solidification process based on the thermodynamic balance theory of Fischer [12].

And there is another theory on the so-called mesomorphic phase generated as a stable intermediate state during induction period of crystallization in the glassy or semi-crystalline states [13-20].

In one of the researches on spherulite nucleation and growth of spherulites, it is reported that PP crystallization is suppressed by rapid cooling, the volume fraction of small monoclinic structure spherulite in smectic crystalline matrix is ca. 20 vol% by Shibayama et al. [21].

Meanwhile, concerning with the solidification process of Fischer, Nitta and Takayanagi [22, 23] proposed the lamellar clustering model with thickness being comparable with the end-to-end chain distance.

On the other hand, on the generation theory of mesomorphic phase, Kaji et al [24-27] reported that the molten isotactic PP transforms into the mesomorphic phase through a spinodal decomposition type separation when it is quenched below 0 ºC with a rate faster than 80 ºC/sec.

There are some articles on the flow-induced crystallization which are focused on obtaining highly transparent PP sheet by the industrial extrusion process under the influence of stress rather than the ideal cooling conditions [28-40].

The purpose of this study is to investigate the effects of the screw geometries, the higher order structure of the higher tacticity PP sheets, the influence of a degree of isotacticity, molecular weight distribution, and the addition of metallocene L-LDPE as crystallization control material contributing to transparency.

And also in order to improve the transparency of isotactic PP sheets, multilayer extrusion was conducted using a resin with lower melt viscosity for the surface layers than one for the core layer.

2. EXPERIMENTAL

Figure 1 shows a schematic diagram of the extrusion process for quick quenching used in the experiments here. A φ65 mm diameter single screw extruder (L / D = 28) and the coat hanger die with 900 mm in width and 2 mm lip openings were used. Extruder barrel temperatures were set as follows: C1 (feed) 200˚C, C2 230˚C, C3 250˚C, C4 (metering) 260˚C. Die sections were set at 260 ˚C and all set temperature were kept constant throughout the experiments.

A direct belt system was used for the cooling system. This take-up device was composed of a mirror finished stainless steel endless belt with 0.65mm in thickness and a mirror finished roll. Illustrated metal rolls were cooled by a chiller unit. The molten resin sheet, which was extruded from the coat hanger die, was nipped and quenched by the mirror finished belt and roll with 18 ℃.

The characteristics of the resin used for the experiment about the influence which it has on the transparency of isotacticity were shown in Table 1. The first character 'H' and 'L' of sample code express the difference in isotacticity. The higher one is set to 'H' and the lower one is set to 'L'. The code 'Q' means quick quenching process and the code 'A' means annealing, after cooling.

The meso pentad fraction was measured by some precedents ^{13}CNMR method to go by [41].

The melting enthalpy ΔH was measured by the differential scanning calorimetry (DSC), and the crystallinity X_C of each sheet was determined from the following equation

$$X_C = \frac{\Delta H}{\Delta H^{\circ}_{PP}} \times 100 \qquad (1)$$

where ΔH is the measured melting enthalpy of the analyzed sample, ΔH°_{PP} is the melting enthalpy of the 100% crystalline phase equal to 164 J/g [42].

The resin characteristics used for the experiment about the influence which it has on the transparency of a molecular weight distribution were shown in Table 2.

The relaxation time was determined by a viscoelasticity data at angular velocity ω of 0.1 rad/s and 1.0 rad/s using a rotary rheometer by Rheometrix Corporation. The conditions for measurement were at the temperature of 175 ºC, φ25 mm diameter of cone and plate and 0.1 rad of the cone angle. The calculation was based on the following equation

$$G^*(i\omega)=G'(\omega)+iG''(\omega) \qquad (2)$$

$$\tau(\omega)=G'(\omega)/\omega G''(\omega) \qquad (3)$$

where G*(iω) is complex modulus of elasticity, G' is storage modulus and G" is loss modulus.

The list of the metallocene L-LDPE used as crystallization control material was shown in Table 3. These L-LDPE resins have density range of 898 to 918 kg/m^3 and the melting point range of 90 to 124 ºC. These metallocene L-LDPE was blended by 10 wt% into PP (MFR 3.0 g/10 min) with 92.5 mol% of meso pentad fraction, respectively. Then they were extruded and quenched by using the equipment shown in Fig. 1. After heat treatment at 120 to 140 ºC, the physical properties of these sheets were measured.

Light scattering patterns were measured photographically and photometrically by using Optorheometer model HRS-100 (ORC Manufacturing Co., Ltd.). The average size of spherulites was calculated from $2\theta_{max}$ of Hv intensity according to Stein's method [43] as follows;

$$R_0 = \frac{4.09}{\frac{4\pi}{\lambda}\sin\theta_{max}} \qquad (4)$$

where R_0 is the radius of spherulite, λ is the wavelength of incident light, $2\theta_{max}$ is the scattering angle which indicates the maximum Hv intensity

Polarizing microscopy was conducted with a Nikon polarized microscope. Wide-angle X-ray diffraction (WAXD) measurement and Small angle X-ray scattering (SAXS) measurement were carried out using model ultra X 18HB (Rigaku Corporation). The powder

diffractometer was used with Ni-filtered Cu-K_α radiation (50 kV, 300 mA, wave-length 0.15418 nm). Transmission electron microscope (TEM) was carried out using Hitachi H800. The thin sliced sample was treated by RuO_4. The refractive index of the sheet sample was measured by using Metricon Model 2010/M Prism Coupler (Metricon Corporation) [44], and the each value was the average of five measured values.

3. RESULTS AND DISCUSSION

3.1 The influence of the screw geometries

The results of extrusion performance with the different screw geometry are shown in Fig. 2 and Table 4 [45]. The screw geometry was selected in order to enable the melt plasticization in the early stage of the extruder under even low shear stress conditions. The screw No. 6 of a straight channel depth screw with a torpedo type barrier section at the middle part of screw was examined. It was excellent in respect to the high transparency and the extrusion stability as a result.

In Fig. 3, the relationship between average melt temperature at the center of the die exit and specific energy consumption at screw speed 150 rpm were plotted. Additionally, the transparency order of melt web was shown in Fig. 3. It was found from the results obtained by experiments of the screw geometry change that high transparency is obtained under the small specific energy consumption and the low melted temperature. In the case of screw No. 5 which was a straight screw of 5 mm in the channel depth, stable melt plasticizing did not occur.

To obtain highly transparent melt web, it is very important not to generate excessive heat owing to the shear stress or the shear rate on the assumption that the unmelted resin particles are not left. And this transparent mechanism is fundamentally different from the “shark skin” generated at the die exit. That is, the “shark skin” is generated at more than a certain limit of shear stress. It means that the lower the melt temperature, the easier the “shark skin” is generated. On the other hand, the lower melt temperature causes higher transparent appearance of melt web depending on the screw geometry.

The straight channel depth screw with a torpedo type barrier achieved the most favorable results for high transparency melt web, and also for the comprehensive evaluation of the extrusion stability, throughput and melt resin temperature. However, in the case of a large size extruder for the production machine, the melt plasticization problem was predicted, and the gently tapered compression screws with a torpedo type barrier were examined in more detail.

In order to secure extrusion stability under the even high throughput condition, the plasticization capacity was improved by the optimization of the screw geometry. And also the low melt temperature was pursued as much as possible. The optimization of the lengths of feed, compression and metering zone was attempted, and also the segment which compulsorily destroyed a solid bed in the entrance section of torpedo was newly investigated. As a result, the screw geometry to satisfy the quality demand was obtained by these optimizations for high transparency and extrusion stability.

3.2 The influence of the isotacticity

In our previous paper, we analyzed the crystallization behavior of high tacticity PP [46]. In this work, the factors for further improvement on the transparency were investigated. In order to consider the influence on the transparency of isotacticity, PP with 92.5 mol% of meso pentad fraction was compared with the high isotacticity PP with 97.9 mol%.

Figure 4 shows micrographs obtained by phase-contrast microscopy of cross section (a) L-Q, (b) H-Q, (c) L-QA and (d) H-QA sheet samples. In the both cases of L-Q and H-Q sheet, a lot of small spherulites [46] were observed especially near the sheet surfaces. Compared with the higher isotacticity PP, even if the sheeting was carried out under the same conditions, the lower isotacticity PP generated the less spherulites. As a result of heat-treating these sheets at 140 ºC, the image of the spherulites in both sheets was obviously weakened by the heat treatment. This shows that the difference of the refractive index of matrix and spherulites became very small by the heat treatment.

The results of having observed the same samples with the polarizing microscopy are shown in Fig. 5. In both sheet samples, the maltese cross

pattern which used to be detected in the case of spherulites could be observed especially near the sheet surfaces, as same as Fig. 4. In the cases of quick quenching samples which the big difference were observed by the phase-contrast microscopy, at a first glance, there were no differences (especially regarding the size and number of spherulites) between quenching sheets and annealed samples by polarizing microscopy. It means that there was no big change from a point of view of a birefringence or an optical anisotropy difference between a matrix and spherulites even by the heat treatment of the quick quenched sheet. This phenomenon was not concerned with their isotacticities.

Figure 6 shows the variation of Vv light scattering intensity distribution curves for L-Q, L-QA, H-Q and H-QA. The Vv light scattering intensity consists of an optical anisotropy ingredient and a density fluctuation ingredient contribution. These data were measured in the direction of the equator where optical anisotropy ingredient contribution was comparatively small. In the cases of both quick quenching samples, it turned out that these relative intensities were quite small by the heat treatment. In particular, the H-Q sheet sample showed the marked downward tendency of relative intensity, and had much effect on transparency by the heat treatment. On the other hand, the relative intensity itself of L-QA sheet is smaller, and it means that the absolute density fluctuation is smaller than that of H-QA sheet. Anyway, by carrying out quenching and heat treatment, density fluctuation was decreased and it is thought that transparency was improved as a result.

Figure 7 shows the variation of Hv light scattering intensity distribution curves for L-Q, L-QA, H-Q and H-QA sheets. The peak angle of Hv scattering means the size of spherical substances, and relative intensity means the number of them. Since intensity peaks were clearly observed in the cases of both L-Q sheet and H-Q sheet, existence of spherulites was suggested. Also this graph shows that the size and number of spherulites didn't change substantially, even if both quick quenched sheets were heat-treated. As observed in Figs. 4 and 5, it turns out clearly that L-Q sheet has markedly smaller numbers and average diameter of spherulites. The relative intensity is proportional to the square of the difference of the polarizability in the optic axis direction and the polarizability in the perpendicular direction to the optic axis [43, 47, 48]. Therefore these results, which relative intensity of both sheets were hardly changed by heat treatment, shows that the anisotropy of polarizability in spherulites did not become small by the heat treatment.

Figure 8 shows the variation of SAXS intensity distribution curves for L-Q, L-QA, H-Q and H-QA. An average long period is calculated from a peak position. The scattering image was isotropic and it means that it was fundamentally a disorderly structure. When both quick quenched sheets were heated at 140 ºC, the peak position of relative intensity shifted to the lower scattering angle and increased.

The transparency and higher order structure of L-Q, L-QA, H-Q and H-QA were summarized in Table 1. As shown in Table 1, it turns out that L-Q sheet which has lower isotacticity, has markedly smaller numbers and average diameter of spherulites. As a result, the obtained sheet was better transparency with low internal haze.

Though the crystallinity of L-QA sheet calculated from the melting enthalpy data of DSC was increased by heat treatment, the size and number of spherulites were almost unchanged. The internal haze of L-QA sheet was dramatically improved by the heat treatment. These phenomena had shown the same behaviors as the higher isotacticity PP.

And it was found that the average correlation length of both sheets calculated by V_v light scattering intensity data were decreased by the heat treatment. Each average long period was increased almost twice. Since the sizes of the spherulites themselves do not have big differences by the heat treatment, these increases of average long period suggest that small crystallites of mesomorphic phase in the matrix merge into some larger structure during meso-α transition process.

From above mentioned matters, it is guessed that the lower isotacticity PP, which is relatively difficult to make chain folded structures, has slower nucleation and growth rate of spherulites, and as a result, the internal haze became better than higher isotacticity PP.

3.3 The influence of the molecular weight distribution

The influence of the molecular weight distribution on transparency was investigated. Table 2 shows the characterization of PP grades used for the experiment. Both grades have same meso pentad fraction and MFR, but different molecular weight distributions. According to GPC data, it turns out that the molecular weight distribution of PP-2 is a little wider than that of PP-1.

The optical characteristics of the sheets quenched by the belt process were shown in Fig. 9 and Table 5. It was found that PP-1 with a narrow molecular weight distribution is relatively better transparency than PP-2. Table 4 shows that especially the outer haze of PP-1 sheet became better, because PP-1 with a narrow molecular weight distribution had shorter relaxation time as shown in Table 2.

3.4 The influence of addition of metallocene L-LDPE as crystallization control material

In previous work, we examined the influence of addition of L-LDPE into PP to modify the impact strength at low temperature [49]. At that time, it was found that the sheet transparency was improved by the addition of the specific L-LDPE. And in the case of PP/L-LDPE=50/50 blend, the notion of fluctuation-induced nucleation/crystallization was reported [50]. Then, the contribution to the transparency by blend of various metallocene L-LDPE with wide range density was investigated.

Figure 10 shows the relationship between the density of blended L-LDPE and total haze. The total haze data which were obtained by quenching and heat treatment at 120 ºC, 130 ºC and 140 ºC were indicated. It was clear that after heat treatment, the transparency of the blended sheets dramatically depended on the density of L-LDPE grade. The L-LDPE grades which showed the excellent transparency of 2% or less of the total haze had the density range of 903 to 905 kg/m^3. The L-LDPE grades with other density range could not achieve the transparency of 2% or less of the total haze. According to the density of added L-LDPE, the suitable heat treatment temperature condition which showed the best transparency was changed.

Figure 11 shows the Hv light scattering patterns of L-Q sheet and L-Q with 10 wt% metallocene L-LDPE (905 kg/m^3) whose transparency was the best. Each average diameter of spherulites was 4.7 μm and 4.1 μm respectively, and in the case of the sheet which contained 10 wt% L-LDPE, the diameter became smaller than that of L-Q. And the addition of 10 wt% L-LDPE has considerably weakened the relative intensity of the scattering pattern, and it means that the number of spherulites dramatically decreased by the addition of L-LDPE into PP.

Figure 12 shows the TEM micrographs of TD cross section in the thickness direction of the sheet which contained 10 wt% L-LDPE (905 kg/m^3). The darker and more heavily stained regions represent the L-LDPE particles. The average particle size of L-LDPE was about 100 nm or less near sheet surface, and it was about 200 nm at the sheet center. Similar phenomena were reported about the blend of PP and rubber particles. It is suggested that the viscosity ratio ($\eta_r = \eta_{dispersed} / \eta_{matrix}$) in blend morphology is very important on the dispersed particle size [51, 52]. It is in the state that the L-LDPE particles were aggregated at the sheet center section where the stress level was relatively low.

The average diameter of spherulites shown in Fig. 11 was 4.1 μm. And also the distributed state of L-LDPE particles in Fig. 12 should be considered. Based on these phenomena, it is thought that L-LDPE particles are incorporated into PP spherulites. Moreover, although Fig. 11 showed that the number of spherulites remarkably decreased by the addition of L-LDPE into PP, the cause was considered because the nucleation and growth velocity of spherulites were suppressed by the existence of these L-LDPE particles.

Figure 13 shows micrographs obtained by phase-contrast microscopy of the sheets in Fig. 11, and Fig. 14 shows micrographs obtained by polarizing microscopy of same sample. As already mentioned, lots of spherulites in L-Q sample were observed relatively near the sheet surface. On the other hand, in the case of L-Q with 10 wt% L-LDPE, very few images of spherulites (the maltese cross pattern was observed in high magnification micrograph of Fig. 14) were observed. It corresponded with the dispersion state of L-LDPE particles in Fig. 12. This results supported the result which the addition of 10 wt% L-LDPE considerably weakened the relative intensity of the scattering pattern in Fig. 11.

Although as above mentioned, the number and size of spherulites remarkably decreased by the addition of L-LDPE into PP, the appearance of

the quick quenching sheet became rather clouded. From this transparency behavior, Fig. 15 paid its attention to the sheet density and the refractive index. In Fig. 15, the typical samples were selected from the various samples in Fig. 10. Figure 15 shows the relationship between sheet density and refractive index for metallocene L-LDPE (898, 905 and 912 kg/m^3) blended PP sheets. These sheets were obtained by quick quenching and then heat treatment at 120, 130 and 140 ºC.

It was found that the refractive index was increased linearly to the sheet density by the various heat treatment conditions. The gradients of the approximated curve of each condition were calculated and shown in Fig. 15. Compared with the PP sheet, the higher the density of added L-LDPE were, the larger the gradient of approximation line became. That is, according to the density of added L-LDPE, the rate of change of the refractive index to the sheet density differed.

Figure 16 shows the relationship between 'absolute value of refractive index difference' at each heat treatment temperature and the total haze based on the data obtained in Fig. 15. The 'absolute value of refractive index difference' was determined from the following equation

Absolute value of refractive index difference = $\left| RI_{PP} - RI_{blended} \right|$ (5)

where RI_{PP} is the refractive index of PP sheet after the heat treatment at T ºC, and $RI_{blended}$ is the refractive index of PP with 10 wt% L-LDPE after the heat treatment at T ºC. Figure 16 shows that the total haze became small in spite of the density of added L-LDPE, when the absolute value of refractive index difference became small.

Figure 17 shows the relationship between the heat treatment temperature and the total haze obtained by 10 wt% additions of L-LDPE with 898, 905 and 912 kg/m^3. In the case of the PP sheet with 898 kg/m^3 L-LDPE, the total haze got worse along with the increase of the heat treatment temperature. On the other hand, in the case of 912 kg/m^3 L-LDPE addition, it turns out that the total haze improved along with the increase of the heat treatment temperature. Moreover, in the case of 905 kg/m^3 L-LDPE addition, it had minimum value of total haze to the heat treatment temperature.

Figure 18 shows the relationship between the heat treatment temperature and the absolute value of refractive index difference. It turns out that the trend pattern of each data was in agreement with Fig. 17.

From the above results, it can be considered the following matter. In the case of 100 % PP sheet, the spherulites worsened the internal haze. And in the case of the L-LDPE addition sheet, although the number and size of spherulites remarkably decreased, the refractive index difference of L-LDPE particles and PP matrix made the internal haze aggravation. That is, in the case of a blend of PP and L-LDPE, because the L-LDPE particles have the different refractive index from PP material, the penetration lights are scattered and it becomes cloudy. Then, the refractive indexes of L-LDPE and PP are approached by the heat treatment, and it can be surmised that the cloudy sheet appearance changes to highly transparent appearance, because the degree of light scattering decreases. However, since the sensitivity of the refractive index to the heat treatment temperature differs in accordance with density of added L-LDPE, the optimum temperature conditions to obtain the best transparency differ.

3.5 Effect for transparency of PP sheets by multilayer sheet extrusion process

In order to improve the transparency of isotactic polypropylene sheet, a multilayer extrusion was conducted using the resin with lower melt viscosity for surface layers than the resin for core layer. As a result, the number of spherulites near the surface decreased dramatically, and furthermore the internal haze of the sheet was improved. The number of spherulites of sheet cross section and the internal haze correlated to each other. The flow velocity distribution, shear rate distribution, and shear stress distribution in a die lip section were calculated using the finite element method. The shear stress in the sheet thickness direction was reduced by laminating resin with low melt viscosity on both surfaces, and therefore it can be surmised that the stress induced crystallization was restrained.

Furthermore, the cooling simulation in a belt quenching process was conducted. The number density of spherulites was set as the response variable, and then the plateau area time of the temperature in each position of the thickness direction and the shear stress were chosen as the independent variable, and the prediction formula

was derived by multiple regression analysis. Moreover, using the obtained formula, some number density of spherulites in various surface layer ratios were predicted, and optimization of multilayer composition was proposed.

4. CONCLUSIONS

In order to improve further the transparency of an isotactic PP sheet obtained by an industrial extrusion quenching process, the important factors were investigated. Especially, the effects of the screw geometries, the higher order structure of the higher tacticity PP sheets, the influence of the isotacticity, a molecular weight distribution, added metallocene L-LDPE and multilayer extrusion over the transparency of PP sheets were investigated.

Even if the sheeting was carried out under the same conditions, the lower tacticity PP generated the less and the smaller size of spherulites, and the better transparent sheet was obtained. In the case of low tacticity PP, the improvement behavior on transparency by heat treatment showed the same tendency as the high tacticity PP. It is guessed that the lower isotacticity PP, which is relatively difficult to make chain folded structures, has slower nucleation and growth rate of spherulites, and as a result, the internal haze became better than higher isotacticity PP.

Concerning the influence of molecular weight distribution on transparency, PP with narrow molecular weight distribution, which has shorter relaxation time, showed better external haze and as a result better transparence.

Moreover, when metallocene L-LDPE was added into PP, the number of generated spherulites and the growth rate of them were restrained by the fine distribution particles of L-LDPE in PP matrix. In the case of addition of L-LDPE with the specific density to PP, the transparency was markedly improved by the heat treatment of quick quenching sheets. According to the density of added L-LDPE, the suitable heat treatment temperature condition which showed the best transparency was changed. Because the sensitivity of the refractive index to the heat treatment temperature differed in accordance with density of added L-LDPE, the optimum temperature conditions to obtain the best transparency differed. In the case of the L-LDPE addition sheet, the refractive index difference of L-LDPE particles and PP matrix made the internal haze aggravation. Then, the refractive indexes of L-LDPE and PP are approached by the heat treatment, and it can be surmised that the cloudy sheet appearance changes to highly transparent appearance, because the degree of light scattering decreases.

5. COMMERCIALIZATION

Thanks to the above mentioned research, we developed the following products without nucleators ;

(1) Super Purelay® is a clear PP sheet having unprecedented transparency, abrilliant surface and extremely high stiffness by utilizing crystallinity controltechnology and glazing process.The main applications are clear boxes and clear packaging for non-food products.(Cosmetic and toletry, stationary, gift, toy, cigarrette, etc.) 3500ton/year.

(2) Purethermo® is a highly transparent PP sheet for thermoforming clear foodcontainers. (blister pack,lid for countainer, portion packs, countainers for desserts,food & daily product) 3000ton/year. As compared with conventional PP sheet with nucleators, it has wide a processwindow for the thermoforming process, good thermoformability and much clearsheet can be produced.

NOMENCLATURE

ΔH: Measured melting enthalpy of analyzed sample (J/g)

ΔH°_{PP} :Melting enthalpy of the 100% crystalline phase (J/g)

X_C:Crystallinity (%)

ω: Angular velocity (rad/s)

$G^*(i\omega)$:Complex modulus of elasticity (Pa)

G' : Storage modulus (Pa)

G": Loss modulus (Pa)

R_0: Radius of spherulite (nm)

λ: Wavelength of incident light (632.8 nm)

$2\theta_{max}$: Scattering angle which indicates the maximum Hv intensity (rad)

RI_{PP} :Refractive index of PP sheet after the heat treatment at T ºC (-)

$RI_{blended}$:refractive index of PP with 10 wt% L-LDPE after the heat treatment at T ºC (-)

REFERENCES

1. W. P. Slichter, E. R. Mandell, *J. Appl. Phys.*, **29**, 1438(1958)
2. G. Natta, *SPE J.*, **15**, 373(1959)
3. R. L. Miller, *Polymer*, **1**, 135(1960)
4. H. W. Wyckoff, *J. Polym. Sci.*, **62**, 83(1962)
5. M. Gletin, R. R. Rahalkar, P. J. Hendra, M. E. A. Cudby, *Polymer*, **22**, 731(1981)
6. P. J. Hendra, J. Vile, H. A. Willis, M. E. A. Cudby, *Polymer*, **25**, 785(1984)
7. P. Corradini, V. Petraccone, C. DeRosa, G. Guerra, *Macromolecules*, **19**, 2699(1986)
8. M. A. Gomez, H. Tanaka, A. E. Tonelli, *Polymer*, **28**, 2227(1987)
9. P. Corradini, C. DeRosa, G. Guerra, V. Petraccone, *Polym. Comm.*, **30**, 281(1989)
10. Z-G. Wang, B. S. Hsiao, S. Srinivas, G. M. Brown, A. H. Tsou, S. Z. D. Cheng, R. S. Stein, *Polymer*, **42**, 7561(2001)
11. J. D. Hoffman, J. I. Lauritzen, *J. Res. Nat. Bur. Std.*, **64**, 297(1961)
12. E. W. Fischer, *Polym. J.*, **17**, 307(1985)
13. M. Imai, K. Mori, T. Mizukami, K. Kaji, T. Kanaya, *Polymer*, **33**, 4451(1992)
14. M. Imai, K. Mori, T. Mizukami, K. Kaji, T. Kanaya, *Polymer*, **33**, 4457(1992)
15. K. Kaji, K. Nishida, T. Kanaya, G. Matsuba, T. Konishi, M. Imai, *Adv, Polym. Sci.*, **191**, 187(2005)
16. T. Konishi, K. Nishida, T. Kanaya, K. Kaji, *Macromolecules*, **38**, 8749(2005)
17. K. Kaji, K. Nishida, T. Kanaya, G. Matsuba, T. Konishi, M. Imai, *Seni Gakkaishi*, **62**, 88 (2006)
18. I. Coccorullo, R. Pantani, G. Titomanlio, *Polymer*, **44**, 307(2003)
19. D. M. Gezovich, P. H. Geil, *Polym. Eng. Sci.*, **8**, 202(1968)
20. D. T. Grubb, D. Y. Yoon, *Polym. Comm.*, **27**, 84(1986)
21. M. Shibayama, K. Katoh, T. Iwamoto, D. Takahashi, S. Nomura, *Polymer J.*, **23**, 837(1991)
22. K. Nitta, M. Takayanagi, *J. Macromol. Sci.-Physics.*, **B42**, 107(2003)
23. K. Nitta, M. Takayanagi, *Polymer J.*, **38**, 757(2006)
24. C. C. Hsu, P. H. Geil, H. Miyaji, K. Asai, *J. Polym. Phys. Ed.*, **24**, 2379(1986)
25. T. Ogawa, H. Miyaji, K. Asai, *J. Phys. Soc. Jpn.*, **54**, 3668(1985)
26. K. Nishida, T. Konishi, T. Kanaya, K. Kaji, *Polymer*, **45**, 1433(2004)
27. T. Konishi, K. Nishida, T. Kanaya, *Macromolecules*, **39**, 8035(2006)
28. F. H. M. Swartjes, G. W. M. Peters, S. Rastogi, H. E. H. Meijer, *International Polymer Processing*, **18**, 53(2003)
29. B. A. G. Schrauwen, L. C. A. van Breemen, A. B. Spoelstra, L. E. Govaert, G. W. M. Peters, H. E. H. Meijer, *Macromolecules*, **37**, 8618(2004)
30. M. H. E. van der Beek, G. W. M. Peters, H. E. H. Meijer, *Macromolecules*, **39**, 1805(2006)
31. L. Balzano, S. Rastogi, G. W. M. Peters, *Macromolecules*, **42**, 2088(2009)
32. J-W. Housmans, R. J. A. Steenbakkers, P. C. Roozemond, G. W. M. Peters, H. E. H. Meijer, *Macromolecules*, **42**, 5728(2009)
33. J. F. Vega, D. G. Hristova, G. W. M. Peters, *J. Therm. Anal. Calorim.*, **98**, 655(2009)
34. Chang-Yu Shen, Ying-Guo Zhou, Guo-Qiang Zheng, Chun-Tai Liu, Jing-Bo Chen, Q. Li, *Polym. Eng. Sci.*, **48**, 2454(2008)
35. R. Su, K. Wang, P. Zhao, Q. Zhang, R. Du, Q. Fu, L. Li, L. Li, *Polymer*, **48**, 4529(2007)
36. J. Zhang, K. Shen, S. Na, Q. Fu, *J. Polym. Sci.*, Part B, **42**, 2385(2004)
37. Y. Wang, B. Na, Q. Fu, Y. Men, *Polymer*, **45**, 207(2004)
38. L. Li, W. H. de Jeu, *Faraday Discuss.*, **128**, 299(2005)
39. C. G. Zhang, H. Q. Hu, D. J. Wang, S. K. Yan, C. C. Han, *Polymer*, **46**, 8157(2005)
40. A. Elmoumni, H. H. Winter, *Rheol. Acta.*, **45**, 793(2006)
41. A. Zambelli, *Macromolecules*, **6**, 925(1973)
42. B. Wunderlich, *Macromolecular Physics, Academic Press: New York*, **vol. 3** (1980)
43. R. S. Stein, M. B. *Rhodes, J. Appl. Phys.*, **31**, 1873(1960)
44. R. Ulrich, R. Torge, *Appl. Opt.*, **12**, 2901(1973)
45. A. Funaki, T. Takubo, T. Kanai, *Polym. Eng. Sci.*, **50**, 420(2010)
46. A. Funaki, T. Kanai, Y. Saito, T. Yamada, *Polym. Eng. Sci.*, **50**, accepted (2010)
47. J. J. van Aartsen, *ONR Technical Rept*. **No. 83**, Polymer Research Inst., University of Massachusetts, Amherst., Mass., USA (1966)
48. J. J. van Aartsen, R. S. Stein, *J. Polym. Sci.*, *A2*, **9**, 295(1971)
49. A. Funaki, Japan Patent 3,751,338(2005)

50. K. Meng, X. Dong, X. Zhang, C. Zhang, C. C. Han, *Macromol. Rapid Commun.*, **27**, 1677(2006)
51. H. P. Grace, *Chem. Eng. Commun.,* **14**, 225(1982)
52. U. Sundararaj, C. W. Macosko, *Macromolecules*, **28**, 2647(1995)

Acknowledgment
Authors would like to express special thanks to Prof.James L. White who gave us very fruitful discussion very kindly during whole his life.
We would like to thank Prof. T.Yamada, Y.Saito, S.Kuratani, M.Nakatsubo, Kanazawa University and Dr.T.Takebe, Idemitsu Kosan, for their excellent techinical support and helpful discussion.

Table 1. Summary of transparency and higher order structure of polypropylene sheets.（thickness ; 300μm）

Sample code	H-Q	H-QA	L-Q	L-QA
Meso pentad fraction (mol%)	97.9	97.9	92.5	92.5
Sheeting process	quick quenching (single belt process)	quick quenching & annealing at 140 ºC	quick quenching (single belt process)	quick quenching & annealing at 140 ºC
ΔH (J/g)	82.6	108.8	76.0	102.5
Crystallinity (%)	50.4	66.3	46.3	62.5
Total haze (%)	19.6	8.5	9.4	5.3
Internal haze (%)	18.3	7.7	6.6	3.6
Outer haze (%)	1.4	0.8	2.8	1.7
Average diameter of spherulites (μm)	6.2	7.5	4.7	4.7
Peak value of H_v scattering intensity $\times 10^{-5}$ (-)	2.94	3.15	0.38	0.64
Average correlation length (μm)	1.74	0.51	1.60	0.64
Average long period (nm)	11.0	19.2	11.6	18.4

Table 2. Characterization of polypropylene grades.

Polypropylene grades		PP-1	PP-2
MFR (g / 10min)		2.9	2.9
Meso pentad fraction (mol%)		91.5	91.5
Melting viscoelasticity	Relaxation time at ω=1 s^{-1} (s)	0.537	0.597
	Relaxation time at ω=0.1 s^{-1} (s)	2.650	2.799
GPC	Mn $\times 10^{-4}$	8.45	7.71
	Mw $\times 10^{-4}$	35.9	35.9
	Mz $\times 10^{-4}$	109	119
	Mw / Mn	4.26	4.66

Table 3. Characterization of metallocene L-LDPE grades as modification materials for transparency

No.	Density (kg/m^3)	MFR (g/10min)	Melting point (ºC)
LL-1	898	3.5	90
LL-2	901	2.0	93
LL-3	902	3.0	98
LL-4	903	3.8	98
LL-5	905	3.5	97
LL-6	907	2.0	100
LL-7	909	2.0	111
LL-8	912	2.0	121
LL-9	918	2.0	124

Table 4. Summary of extrusion performance for each screw geometry

Screw No.	Screw Geometry	Extrusion Stability Fluctuation range at screw tip (MPa)	Transparency	Throughput at 150rpm (Kg/H)	Specific Energy Consumption at 150rpm (WH/Kg)	Melt Temperature at 150rpm (℃)
1	Low compression, deep metering channel depth	± 18.5	4	54	0.242	248
2	Low compression, shallow metering channel depth	± 0.3	2	39	0.314	252
3	Low compression, metering with mixer	± 0.3	1	43	0.292	261
4	Straight channel depth (4mm)	± 5.3	5	43	0.169	237
5	Straight channel depth (5mm)	± 9.5	3	57	0.170	228
6	Straight channel depth (4mm) with topido type barrier (δ=1.0mm, L=50mm)	± 0.3	5	43	0.178	245
7	Straight channel depth (4mm) with topido type barrier (δ=1.0mm, L=150mm)	± 0.3	1	43	0.241	256
8	Straight channel depth (4mm) with topido type barrier (δ=0.5mm, L=50mm)	± 0.4	1	45	0.217	254

Definition of transparency : Excellent =5, Very Good=4, Good=3, Fair=2, Poor=1

Table 5. Results of transparency and gloss of polypropylene sheets made of PP1 and PP2 grades

(Thickness 300μm)

	Total haze (%)	Internal haze (%)	Outer haze (%)	Gloss (%)	
				Roll side	Belt side
PP1 sheet	3.0	1.6	1.4	143	136
PP2 sheet	3.5	1.7	1.8	137	128

FIGURES

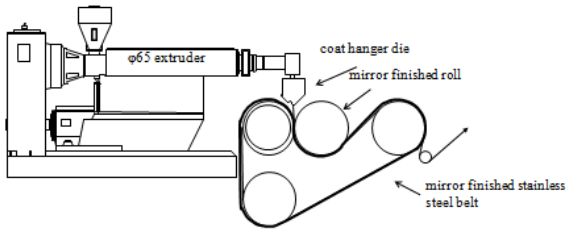

FIG. 1. Schematic diagram of extrusion sheeting system (single belt quick quenching process)

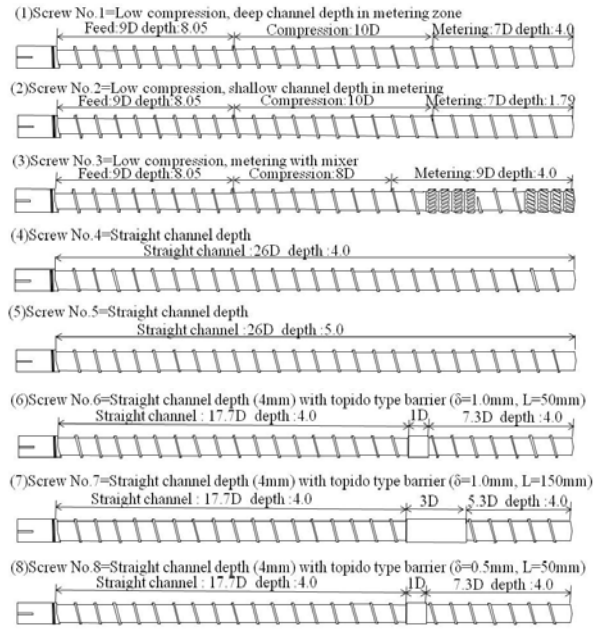

FIG. 2. Schematic representation of screw geometries, lengths expressed in extruder screw diameters

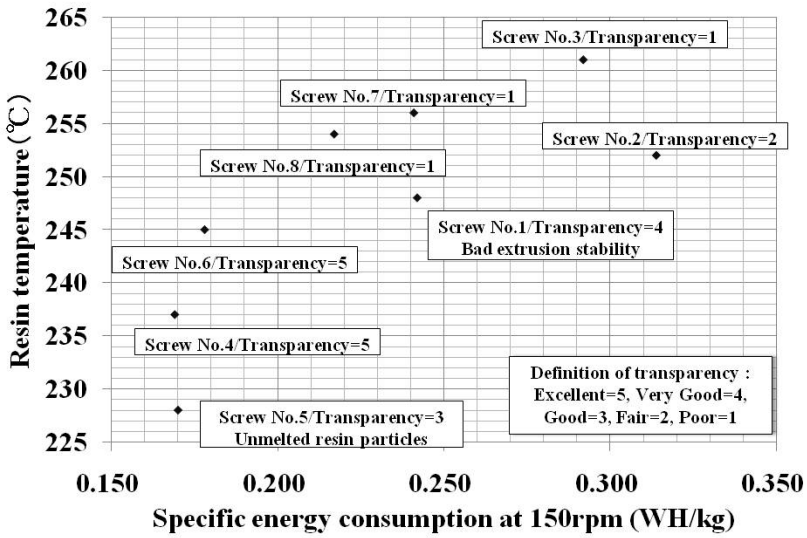

FIG. 3. The relationship between average melt temperature and specific energy consumption at 150rpm for each screw

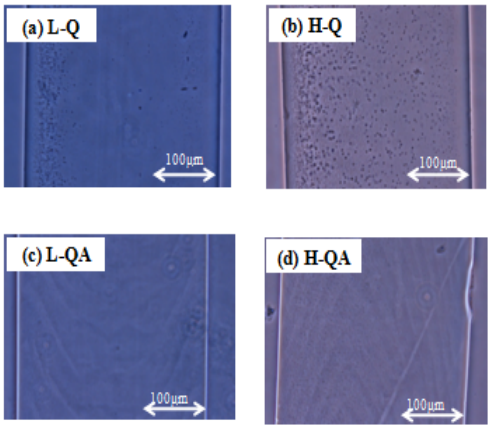

FIG. 4. Micrographs obtained by phase-contrast microscopy of cross sections of (a) L-Q, (b) H-Q, (c) L-QA and (d) H-QA sheets

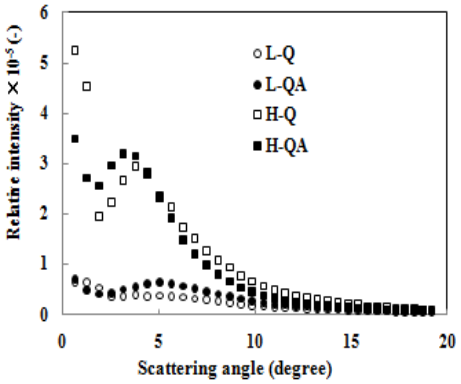

FIG. 7. Variation of H_v light scattering intensity distribution curves for L-Q, L-QA, H-Q and H-QA

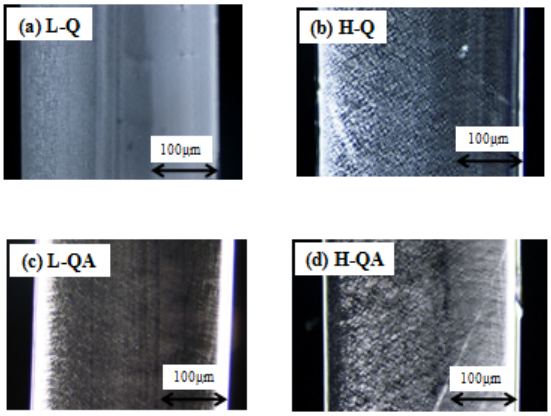

FIG. 5. Micrographs obtained by polarizing microscopy of cross sections of (a) L-Q, (b) H-Q, (c) L-QA and (d) H-QA sheets

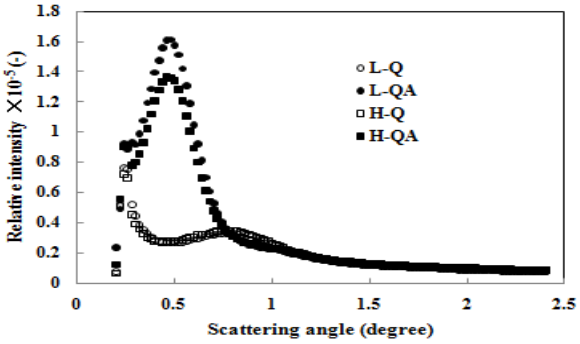

FIG. 8. Variation of SAXS intensity distribution curves for L-Q, L-QA, H-Q and H-QA

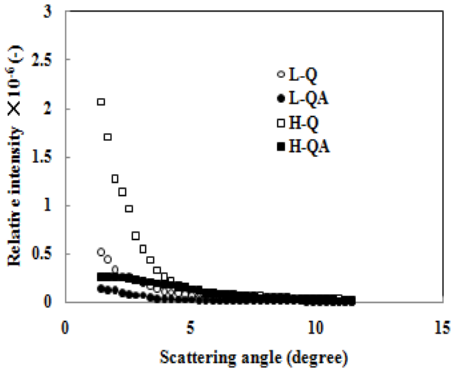

FIG. 6. Variation of V_v light scattering intensity distribution curves for L-Q, L-QA, H-Q and H-QA.

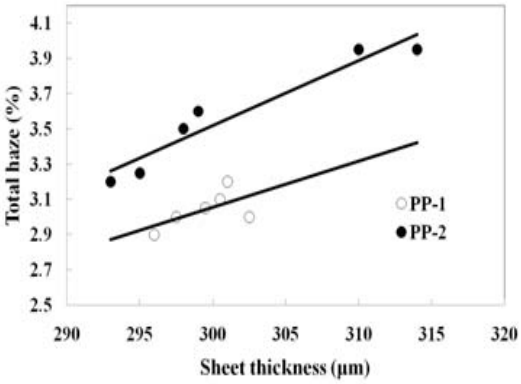

FIG. 9. Effect of molecular weight distribution on sheet transparency, where (a) PP-1 (Mw/Mn=4.26), (b) PP-2 (Mw/Mn=4.66)

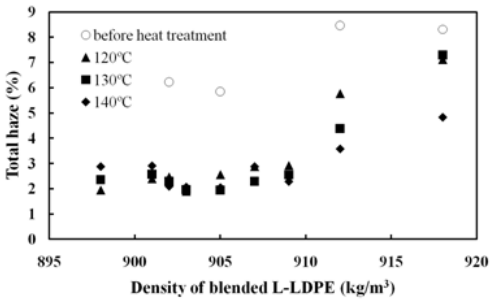

FIG. 10. Effect of density of blended metallocene L-LDPE into PP on sheet transparency for different heat treatment temperatures

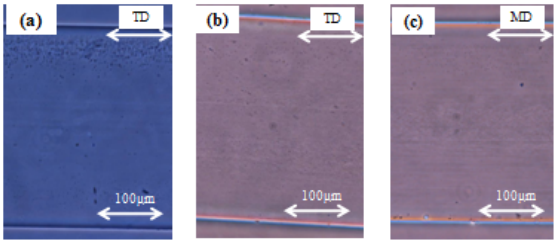

FIG. 13. Micrographs obtained by phase-contrast microscopy of cross sections of (a) L-Q, (b) and (c) L-Q with 10 wt% L-LDPE (ρ = 905 kg/m^3) sheets

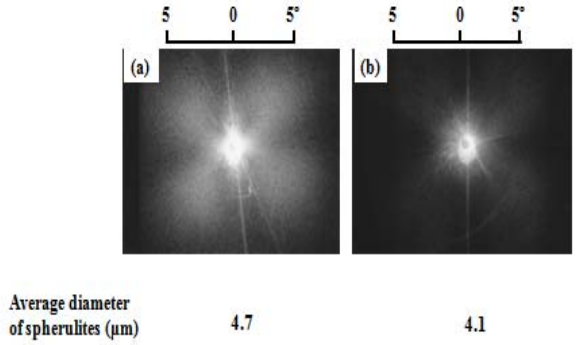

FIG. 11. H_v light scattering patterns for (a) L-Q and (b) L-Q with 10 wt% L-LDPE (ρ = 905 kg/m^3) sheets

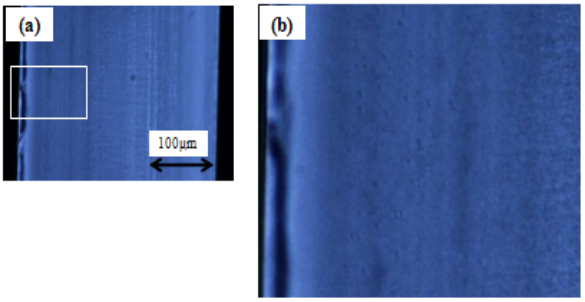

FIG. 14. Micrographs obtained by polarizing microscopy of cross sections of (a) L-Q with 10 wt% L-LDPE (ρ = 905 kg/m^3) sheets and (b) its high magnification micrograph

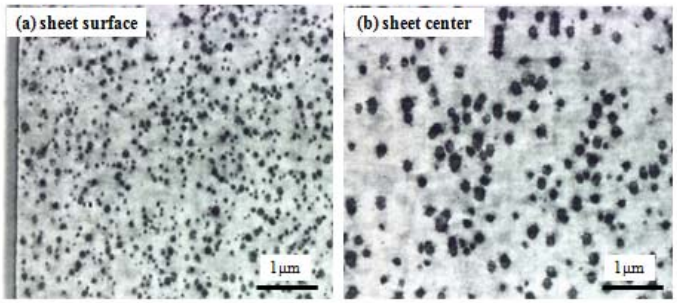

FIG. 12. Micrographs obtained by transmission electron microscopy of TD cross sections of L-Q with 10 wt% L-LDPE (ρ = 905 kg/m^3) sheet

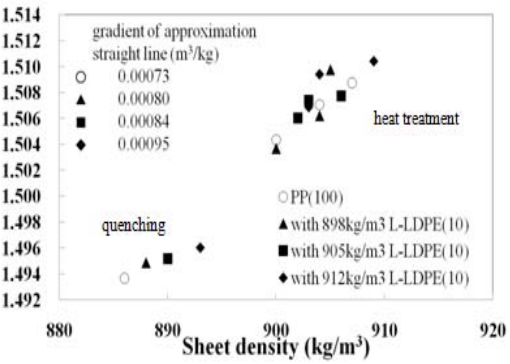

FIG. 15. Relationship between sheet density and refractive index for various metallocene L-LDPE blended PP sheets

.

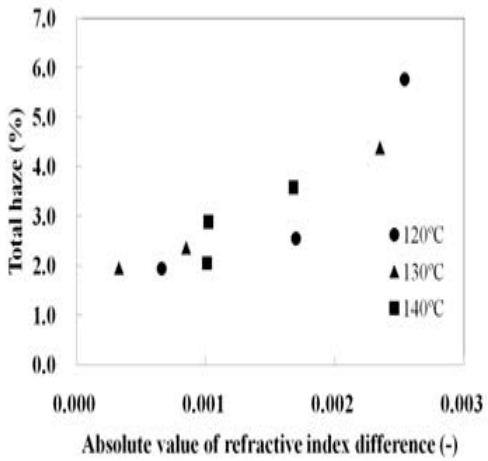

FIG. 16. Relationship between transparence and absolute value of refractive index difference of PP sheet and L-LDPE blended sheet as a function of heat treatment temperatures

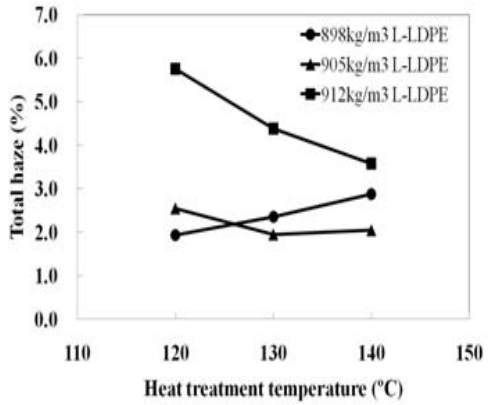

FIG. 17. Relationship between transparence and heat treatment temperatures for various metallocene L-LDPE blended PP sheets

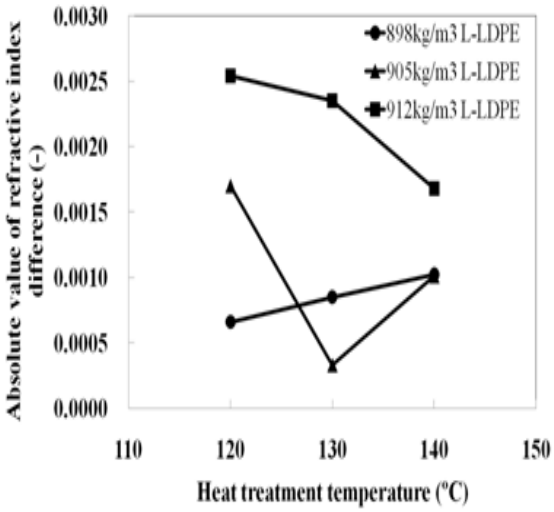

FIG. 18. Relationship between absolute value of refractive index difference of PP sheet and L-LDPE blended sheet and heat treatment temperatures for various metallocene L-LDPE blended PP sheets